



Ion Transport in Hydroxide Conducting Block Copolymers

Journal:	<i>Molecular Systems Design & Engineering</i>
Manuscript ID	ME-PER-02-2019-000022.R1
Article Type:	Perspective
Date Submitted by the Author:	28-Mar-2019
Complete List of Authors:	Elabd, Yossef; Texas A&M University College Station

SCHOLARONE™
Manuscripts

Design, System, Application Statement:

Hydroxide ion conducting block copolymers have the potential to possess the multiple properties required for anion exchange membranes to enable long-lasting alkaline fuel cell performance, and therefore can accelerate the advancement of the alkaline fuel cell, a low-cost alternative to the well-adopted commercial proton exchange membrane fuel cell. In this paper, an overview of hydroxide ion transport (a property that is proportional to fuel cell performance) in block copolymers will be presented and the subsequent impact of block copolymer morphology on ion transport (conductivity), where the careful design of block copolymer chemistry and chain architecture can accelerate hydroxide ion transport.

Ion Transport in Hydroxide Conducting Block Copolymers

*Yossef A. Elabd**

Department of Chemical Engineering, Texas A&M University, College Station, TX 77843

*To whom correspondence should be addressed; email: elabd@tamu.edu

ABSTRACT: Hydroxide ion conducting block copolymers have the potential to possess the multiple properties required for anion exchange membranes to enable long-lasting alkaline fuel cell performance, and therefore can accelerate the advancement of the alkaline fuel cell, a low-cost alternative to the well-adopted commercial proton exchange membrane fuel cell. In this paper, an overview of hydroxide ion transport (a property that is proportional to fuel cell performance) in block copolymers will be presented and the subsequent impact of block copolymer morphology on ion transport (conductivity), where the careful design of block copolymer chemistry and chain architecture can accelerate hydroxide ion transport.

1. Introduction

In 2011, Elabd and Hickner¹ published a review on block copolymers for fuel cells. At that time, the focus of their work was on proton conducting sulfonated block copolymers as solid separators for proton exchange membrane fuel cells (PEMFCs). This review highlighted the benefit of the block copolymer chain architecture, wherein having two chemistries sequentially coupled on a molecular level allows for the synergistic conjoining of two orthogonal properties (high ion

transport (from the ionic polymer) and high mechanical strength (from the non-ionic polymer)). This is due to the self-assembly of two distinct polymers into well-defined nanostructures with tunable morphology and domain size. Specifically, results on sulfonated block copolymers revealed that morphology type, orientation, and domain size all had a significant impact on proton conductivity (where higher proton conductivity or lower membrane resistance results in higher fuel cell power). Additionally, a number of studies showed significantly higher proton conductivities in sulfonated block copolymers compared to their analogous random copolymers suggesting that the confinement and organization of covalently attached sulfonic acid moieties within a block copolymer ordered nanostructure accelerates proton transport across the material. Therefore, block copolymers have been a widely popular approach in the development of lower cost PEMs as a possible replacement to ubiquitously used commercial fluorinated Nafion PEM.

Also, in the Elabd and Hickner paper,¹ the development of hydroxide conducting block copolymers as solid separators for application in alkaline fuel cells (AFCs) was briefly mentioned. At the time of their paper, there were only two reports on the development of hydroxide conducting block copolymers for AFCs.^{2,3} Since this time, there has been a significant increase in the number of reports on hydroxide conducting block copolymers for AFCs.⁴⁻⁵⁵ The accelerated growth in the development of hydroxide ion conducting polymers and block copolymers as solid separators or anion exchange membranes (AEMs) for AFCs is due to the potential for solid-state AFCs to replace current well-adopted commercial PEMFCs. Dissimilar to PEMFCs, which require platinum as a catalyst due the sluggish oxygen reduction electrokinetics in acidic environments, AFCs can produce high power densities at similar temperatures with non-noble metal catalysts (*e.g.*, nickel) due to their facile oxygen reduction electrokinetics in basic environments.⁵⁶ Therefore, AFCs hold the promise of a lower cost fuel cell, however, for a commercial long-lasting

AFC to be realized, it requires an AEM with a combination of properties, including sufficiently high hydroxide ion conductivity (*i.e.*, $> 10 \text{ mS cm}^{-1}$; high hydroxide conductivity or lower membrane resistance results in higher alkaline fuel cell power⁵⁷), adequate mechanical properties (*i.e.*, high modulus; limited membrane swelling from water sorption), and high chemical stability at high pH conditions. The constraint of multiple required orthogonal properties has motivated the significant increase in published work on hydroxide conducting block copolymers, where the reports to date have synthesized various hydroxide conducting block copolymers and characterized their properties, including morphology, hydroxide ion conductivity, water sorption, mechanical properties, and alkaline chemical stability.

The focus of this paper is to highlight key observations regarding hydroxide ion transport in block copolymers, their subsequent transport-morphology relationships, and their similarities and dissimilarities when comparing to proton transport in sulfonated block copolymers. This paper will also compare hydroxide ion transport in block copolymers to analogous random copolymers, analogous polymer blends, analogous homopolymers, and discuss the impact of morphology type and microdomain size on hydroxide ion transport.

2. General Observations on Hydroxide Ion Transport in Block Copolymers

Table 1 lists many of the hydroxide conducting block copolymers that have been developed since 2011 and their hydroxide ion conductivity and ion exchange capacity (IEC) or ion concentration or density. Figure 1 shows the chemical structures of several of the hydroxide conducting block copolymers in Table 1.

Table 1. Examples of Hydroxide Conducting Block Copolymers.

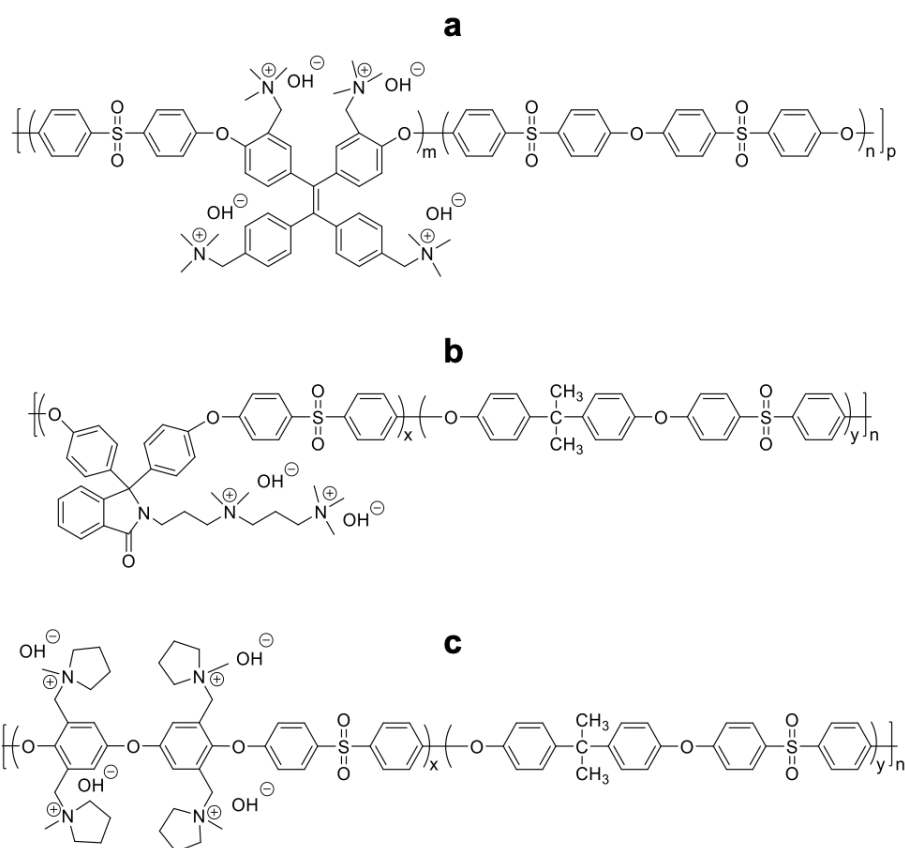
Block Copolymer	IEC^a (meq g⁻¹)	Hydroxide Conductivity (mS cm⁻¹)	Condition^b	Ref.
# Xylylene ionene-based diblock copolymer with main chain ammonium cations	2.34	50	liquid water, 25 °C	4
# Poly(arylene ether sulfone)-based diblock copolymer with pendant ammonium cations	1.93	144	liquid water, 80 °C	5
# Poly(arylene ether sulfone)-based diblock copolymer with pendant ammonium cations	1.95	46.3	liquid water, 60 °C	6
* Poly(styrene)-based diblock copolymer with pendant ammonium and imidazolium cations	^g	<i>ca.</i> 20 ^c	liquid water, 75 °C	13
# Cardo poly(arylene ether sulfone)-based diblock copolymer with pendant imidazolium cations	1.45	100	liquid water, 80 °C	10
* Crosslinked poly(styrene)-based diblock copolymer with pendant ammonium cations	1.65	120	liquid water, 60 °C	9
# Poly(arylene ether sulfone)-based diblock copolymer with pendant ammonium and imidazolium cations	1.30	110	liquid water, 80 °C	11
# Poly(phenylene oxide) diblock copolymer with pendant ammonium cations	1.27	84	95% RH, 80 °C	12
# Poly(arylene ether sulfone)-based diblock copolymer with pendant ammonium cations	1.38	37.7	liquid water, 60 °C	8
* Poly(styrene)-based diblock copolymer with pendant ammonium cations	1.36	12.55	90% RH, 80 °C	14
* Poly(methacrylate)-based diblock copolymer with pendant imidazolium cations	1.4	25	90% RH, 80 °C	15
* Poly(styrene)- <i>b</i> -poly(isoprene)-based diblock copolymer with pendant ammonium cations	0.95	25	liquid water, ambient	17
* Poly(methacrylate)-based diblock copolymer with pendant imidazolium cations	1.44	64.85 ^d	90% RH, 80 °C	22
# Poly(arylene ether sulfone)-based diblock copolymer with pendant ammonium cations	1.57	69.5	liquid water, 80 °C	19

# Poly(arylene ether)-based diblock copolymer with pendant ammonium, imidazolium and pyrrolidinium cations	1.9	<i>ca.</i> 60	liquid water, 80 °C	21
# Poly(arylene ether sulfone)-based diblock copolymer with pendant ammonium cations	1.89	29.30	100% RH, 80 °C	16
# Poly(arylene ether sulfone)- <i>b</i> -poly(phenylene oxide)-based triblock copolymer with pendant ammonium cations	1.83	129	liquid water, 80 °C	18
# Fluorinated poly(phenylene oxide)-based diblock copolymer with pendant ammonium cations	2.1	62	liquid water, 80 °C	23
* Poly(styrene)-based diblock copolymer with pendant ammonium cations	1.72	33	95% RH, 50 °C	26
* Poly(ethylene)- <i>b</i> -poly(styrene)-based diblock copolymer with pendant ammonium cations	1.92	73	liquid water, 60 °C	24
* Poly(styrene)- <i>b</i> -poly(isoprene)-based diblock and triblock copolymers with pendant benzyl phosphonium cations	0.45	20.6 ^c	95% RH, 80 °C	33
# Fluorinated poly(arylene ether)-based diblock copolymer with pendant ammonium cations	1.30	119.7	liquid water, 80 °C	30
* Fluorinated poly(styrene)-based diblock copolymer with pendant ammonium cations	0.49	12.2	liquid water, 70 °C	29
* Poly(styrene)-based diblock copolymer with pendant pyridinium cations	1.42	45 ^c	liquid water, 20 °C	27
# Cardo poly(arylene ether sulfone)-based diblock copolymer with pendant bis-ammonium cations	1.86	52.1	liquid water, 80 °C	28
* Poly(styrene)- <i>b</i> -poly(ethylene- <i>r</i> -butylene)-based triblock copolymer with pendant ammonium cations	1.23	56.4	liquid water, 80 °C	39
# Poly(arylene ether)-based diblock copolymer with pendant ammonium cations	1.4	60 ^c	100% RH, 80 °C	38
# Poly(arylene ether sulfone)-based diblock copolymer with pendant tetra-pyrrolidinium cations	2.07	68.0	liquid water, 80 °C	35
# Poly(arylene ether sulfone)-based diblock copolymer with main chain piperdinium cations	1.95	102	liquid water, 80 °C	41
* Poly(tert-butyl styrene)- <i>b</i> -poly(ethylene- <i>r</i> -butylene)- <i>b</i> -poly(methyl	0.94	60 ^d	95% RH, 90 °C	37

styrene)-based pentablock terpolymers with pendant ammonium cations				
* Poly(ethylene)- <i>b</i> -poly(styrene)-based diblock copolymer with pendant ammonium cations	1.08	34 ^e	95% RH, 90 °C	40
# Poly(arylene ether ketone)-based diblock copolymer with pendant ammonium cations	1.54	37.6	liquid water, 80 °C	36
* Crosslinkable poly(styrene)-based triblock copolymer with pendant ammonium cations	2.11	46.1	liquid water, 20 °C	44
* Poly(styrene)- <i>b</i> -poly(ethylene- <i>r</i> -butylene)-based triblock copolymer with pendant ammonium cations	1.93	136	liquid water, 70 °C	42
* Poly(styrene)-based diblock copolymer with main chain pyrrolidinium cations	1.78	80	liquid water, ambient	34
# Poly(arylene ether sulfone)-based diblock copolymer with pendant ammonium cations	1.10	66.1	liquid water, 80 °C	43
* Poly(<i>tert</i> -butyl styrene)- <i>b</i> -poly(ethylene- <i>r</i> -butylene)- <i>b</i> -poly(methyl styrene)-based pentablock terpolymers with pendant pyrrolidinium cations	^g	44	liquid water, 60 °C	49
# Poly(arylene ether sulfone)-based diblock copolymer with pendant ammonium and imidazolium cations	2.11	63	liquid water, 80 °C	50
# Poly(arylene ether sulfone)-based diblock copolymer with pendant imidazolium cations	1.30	98.7	liquid water, 80 °C	53
* Crosslinkable poly(styrene)-based diblock copolymer with pendant ammonium cations	1.42	13.1	liquid water, ambient	51
# Crosslinkable poly(arylene ether sulfone)-based diblock copolymer with pendant ammonium cations	1.42	178.77	100% RH, 100 °C	46
# Fluorinated poly(arylene ether)-based diblock copolymer with pendant imidazolium cations	1.25	35	liquid water, ambient	52
* Fluorinated poly(styrene)-based diblock copolymer with pendant ammonium cations	4.27	86.1	liquid water, ambient	55
# Fluorinated poly(arylene ether)-based diblock copolymer with pendant ammonium, quinuclidium and benzyl phosphonium cations	1.42	101.2	liquid water, 80 °C	47

* Poly(styrene)- <i>b</i> -poly(butadiene)-based triblock copolymer with pendant ammonium cations	1.10	20.5 ^f	liquid water, 80 °C	48
# Poly(arylene ether sulfone)-based diblock copolymer with pendant ammonium cations	1.15	86.3	liquid water, 80 °C	54

aromatic backbone; * aliphatic backbone; ^a IEC = ion exchange capacity (meq g⁻¹); ^b condition of conductivity experiment; ^c chloride ion conductivity; ^d bromide ion conductivity; ^e fluoride ion conductivity; ^f bicarbonate ion conductivity; ^g not reported



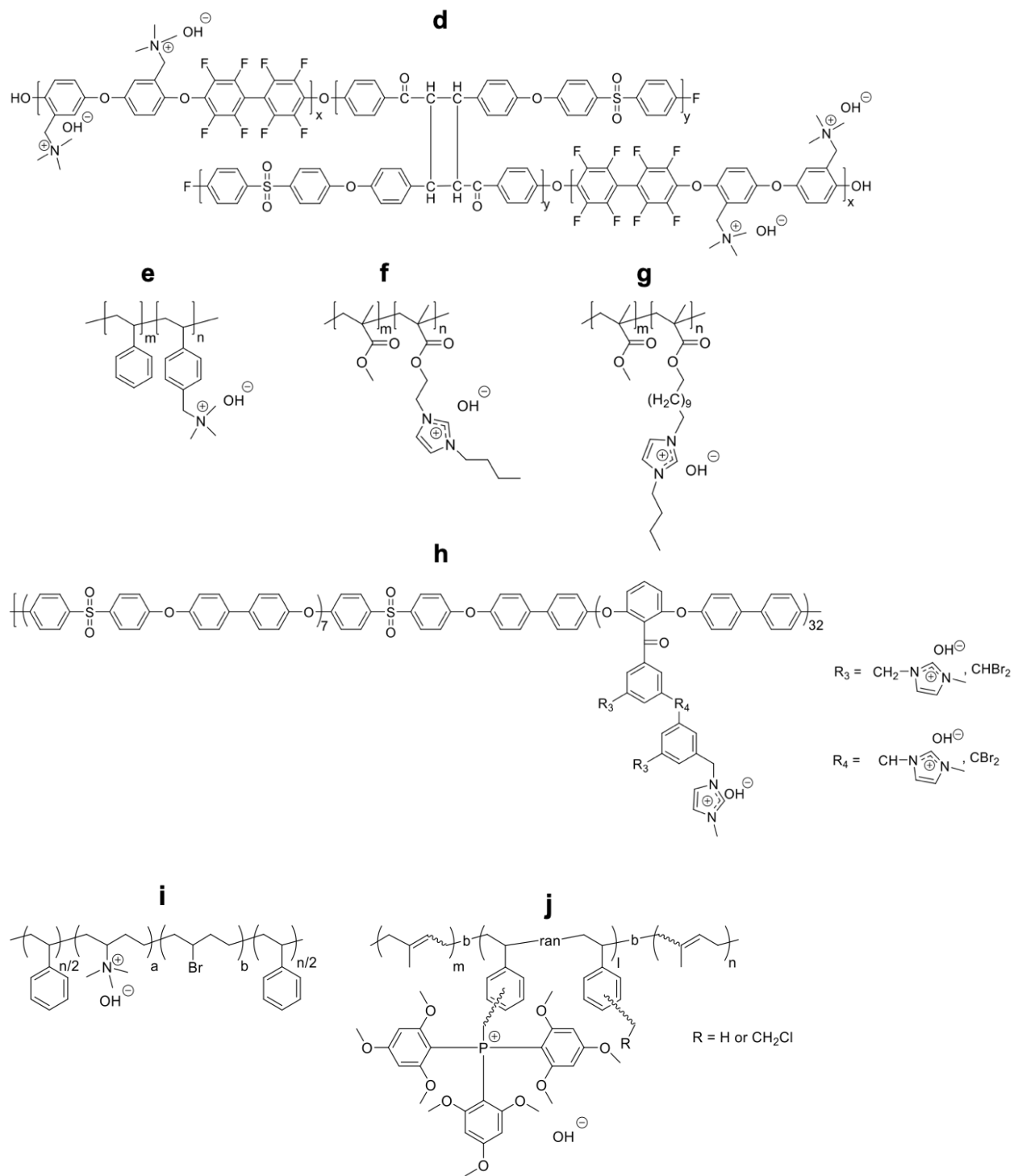


Figure 1. Examples of hydroxide ion conducting block copolymer chemical structures.^{16, 28, 35, 46, 26,15,25, 32,53,48,33}

Several general observations when examining these works, include (1) ion transport mechanisms or trends, (2) differences in backbone chemistry, (3) variations in cation chemistry, and (4) variations in anion chemistry (*i.e.*, anions other than hydroxide). In almost all of these studies, ion conductivity increased with increasing water uptake or hydration number (moles of water per moles of covalently attached ion) and/or IEC and also increased with increasing temperature. Increasing conductivity with increasing water content is similar to what has been observed in proton conducting sulfonated block copolymers (and other sulfonated polymers)¹ and also other hydroxide conducting polymers.⁵⁸ This highlights the water-assisted transport mechanism that is common among proton conducting polymers. Also, it has been shown that hydroxide conductivity in block copolymers scales with volume fraction of water according to percolation theory²⁵ similar to proton conducting sulfonated block copolymers (and other sulfonated polymers, such as Nafion).^{1, 59, 60} Hibbs, Hickner, Cornelius and coworkers⁵⁸ directly compared the proton and hydroxide water-assisted transport properties of a PEM and AEM, respectively. In addition to water, in all of these studies, ion conductivity follows an Arrhenius behavior as a function of temperature at high humidities and/or saturated in liquid water (*i.e.*, a thermal hopping motion facilitated by the water-assisted transport mechanism). This is also similar to what has been observed in sulfonated block copolymers (and other sulfonated polymers).^{59, 60} This differs from lithium ion transport in polymers (under dry conditions), where ion transport is dictated by the segmental dynamics of the polymer chains and follows a Vogel-Fulcher-Tammann (VFT) behavior.⁶¹ Therefore, hydroxide conducting block copolymers are similar to proton conducting block copolymers in that ion transport is a strong function of water content and temperature and therefore these are critical parameters that dictate fuel cell performance.

Another general observation is in regard to the differences in the block copolymer backbone chemistry, which typically fall into one of two categories: aromatic or aliphatic (noted in Table 1). Aromatic backbone block copolymers were typically based on poly(arylene ether) or poly(arylene ether sulfone) chemistry, while aliphatic block copolymers were typically found to be mostly based on poly(styrene) chemistry. Similar to what has been observed in sulfonated block copolymers,¹ the morphology of aromatic backbone block copolymer exhibited microphase separation (or nanoscale morphology) between ion-rich and ion-poor domains, but did not exhibit ordered periodic structures, whereas many of the aliphatic backbone block copolymers exhibited microphase separated ordered periodic structures (*e.g.*, cylinders, lamellae). Although, periodic morphology type can influence ion conductivity in hydroxide block copolymers (discussed more later), overall, high hydroxide ion conductivity in both aromatic and aliphatic backbone block copolymers have been reported (see Table 1), therefore, periodicity is not required for high hydroxide ion conductivity. These results are similar to those reported for proton conductivity in sulfonated block copolymers.¹

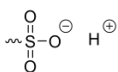
One should also note when reviewing Table 1 and Figure 1, the variety in covalently tethered cations that have been explored (Figure 2). This differs from most of the work on proton conducting polymers, where covalently tethered sulfonic acid is ubiquitous in this field of study. An exploration into different cation chemistries for hydroxide conducting polymers is motivated by the application to AFCs, where high alkaline chemical stability is required for long-lasting AFC performance (*i.e.*, must withstand the AFC environment of high pH at 80 °C). Because of the high nucleophilicity and basicity of the hydroxyl ions produced in the AFC, a variety of known degradation pathways can be triggered in the polymer for the covalently tethered cation, the polymer backbone, and the linker between backbone and cation.⁶²⁻⁶⁴ Among all the hydroxide

conducting block copolymers synthesized (Table 1), benzyl trimethylammonium is a commonly used cation, but has also shown to degrade in alkaline conditions over time, which has spurred the exploration of alternative cation types, such as imidazolium, pyrrolidinium, piperidinium, guanidinium, and phosphonium (Figure 2).⁶⁵ Several investigators synthesized hydroxide conducting block copolymers with various covalently attached cations on the same backbone.^{21,47} In both of these studies, both the conductivity and water uptake scaled with cation type: ammonium > imidazolium > pyrrolidinium and ammonium > phosphonium > quinuclidium, respectively. The authors noted variations in cation size and hydrophilicity for these differences. However, differences in block copolymer microdomain size and cation pK_b could influence ion transport properties as well. One study by Balsara and coworkers¹³ reveals a weak dependency on domain size between to block copolymers with two different cations (trimethylammonium *vs.* butylimidazolium), but reveals a more significant difference in equilibration time between the two block copolymers when exposed to water. In proton conducting sulfonated polymers, it is well known that the differences in pK_a between benzyl sulfonic acid and fluoroether sulfonic acid results in a different proton conductivity-hydration number relationship. Future studies on hydroxide conducting block copolymers with various covalently tethered cations would be of interest.

Another area of dissimilarity between proton conducting and hydroxide conducting polymers is the counter anion. Typically, for proton conducting sulfonated polymers, after ion exchange to proton or acid form, this form of the polymer is known to be stable at ambient conditions. However, for hydroxide conducting polymers, after ion exchange to hydroxide ion form, this form of the polymer is typically not stable in air over time, where trace amounts of carbon dioxide in the air will effectively ion exchange the polymer from hydroxide ion form to carbonate ion form and then

to bicarbonate ion form. Therefore, great care must be taken during ion exchange to hydroxide ion form and subsequently measuring hydroxide ion conductivity, where both processes (and the transfer between them) require careful purging with a gas that contains no carbon dioxide (typically ultra-pure argon). An alternative is to ion exchange the polymer to bicarbonate ion form or another halide anion (*e.g.*, chloride, bromide, fluoride) form and measure the conductivity in this anion form (which is stable under ambient conditions) and assume the conductivity scales with ion size and that the ion transport trends are similar to the polymer in hydroxide ion form. Therefore, several of the studies on hydroxide ion conducting block copolymers have reported bicarbonate, chloride, bromide, or fluoride ion conductivity as noted in Table 1.

Proton Conducting Anion



Hydroxide Conducting Cations

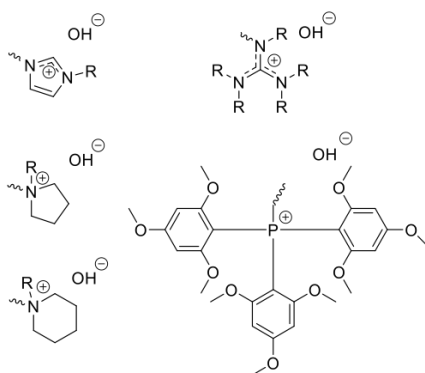


Figure 2. Proton conducting sulfonic acid anion *versus* examples of various hydroxide conducting cations.

3. Block Copolymers *versus* Random Copolymers

Several investigators have synthesized hydroxide ion conducting block copolymers and their analogous random copolymers and reported on their subsequent transport-morphology

relationships.^{15, 16, 28, 35, 46, 66} Previously, similar studies have also been conducted on sulfonated block copolymers¹ and other single ion conducting block copolymers,⁶¹ where the ion conductivity was always reported to be several factors (or even orders of magnitude) higher in block copolymers compared to their analogous random copolymers due to the microphase separated morphologies in block copolymers and their ability to localize ion concentration and movement in an ordered structure.

Figure 3 provides several examples of hydroxide ion conductivity in block copolymers and their analogous random copolymers.^{6, 25, 28, 41} Figure 3a shows the temperature-dependent hydroxide conductivity of poly(arylene ether sulfone) block (bQAPDHTPE) (see chemical structure in Figure 1a) and random (rQAPDHTPE) copolymers with 4,4'-(2,2-diphenylethenylidene) and quaternary ammonium cations.¹⁶ In this study, the hydroxide ion conductivity at 80 °C and 100% RH is higher in the block copolymer (21.37 mS cm⁻¹) compared to the random copolymer (17.91 mS cm⁻¹) when both polymers have the same IEC (1.6 meq g⁻¹). Figure 3a also shows that the higher conductivity is persistent at all temperatures measured (40, 60, 80 °C). The investigators attribute this difference to the phase separated morphology between hydrophilic/hydrophobic domains in the block copolymer as evidenced by atomic force microscopy (AFM).

Figure 3b shows the temperature-dependent hydroxide ion conductivity of cardo poly(arylene ether sulfone) block (QBPEs) (see chemical structure in Figure 1b) and random (QRPEs) copolymers with bis-quaternary ammonium cations. Over this entire temperature range (30 – 80 °C; in liquid water), the hydroxide ion conductivity of the block copolymer is higher than the analogous random copolymer, where both polymers have the same IEC (1.93 mS cm⁻¹). For example, the conductivity at 60 °C is 40.5 and 30.0 mS cm⁻¹ for the block and random copolymers, respectively. The authors attribute this higher conductivity to the formation of microphase

separation in the block copolymer measured by small-angle X-ray scattering (SAXS) and transmission electron microscopy (TEM). More specifically, they suggest that the continuous and ion-rich hydrophilic domains of the block copolymer form interconnected ion transport channels that effectively improves the transport of hydroxide ions.

Figure 3c shows the temperature-dependent hydroxide ion conductivity of poly(arylene ether sulfone) block (QQBPES) (see chemical structure in Figure 1c) and random (QQRPEs, DQRPEs) copolymers with di- (DQRPEs) and tetra-pyrrolidinium (QQRPEs, QQBPES) cations. Similar to other studies, the conductivity of the block copolymer (QQBPES) (68 mS cm^{-1} ; $80 \text{ }^\circ\text{C}$) is higher than its analogous random copolymer (QQRPEs) (36 mS cm^{-1} ; $80 \text{ }^\circ\text{C}$) at the same IEC (2.2 meq g^{-1}) over the entire temperature range investigated ($30 - 80 \text{ }^\circ\text{C}$). The authors attribute this to the block copolymer morphology, where a phase separated connected network of ionic clusters were observed with SAXS and TEM.

Figure 3d shows the temperature-dependent hydroxide ion conductivity of crosslinkable fluorinated poly(arylene ether sulfone) block (QPPAES, XQPPAES) (see chemical structure in Figure 1d) and random (QrPAE, XQrPAE) copolymers with bis-quaternary ammonium cations. Again, the block copolymer (QPPAES-15-11) exhibits higher hydroxide conductivity than its analogous random copolymer (QrPAE-60) at the same IEC (1.4 meq g^{-1}) over the entire temperature range studied ($20 - 100 \text{ }^\circ\text{C}$). Specifically, at $100 \text{ }^\circ\text{C}$, the block copolymer (QPPAES-15-11) and its crosslinked version (XQPPAES-15-11) possessed conductivities of 208.73 and $178.77 \text{ mS cm}^{-1}$, respectively, while the analogous random copolymer (QrPAE-60) and its crosslinked version (XQrPAE-60) possessed conductivities of 59.12 and 52.51 mS cm^{-1} , respectively; an approximate four-fold difference in conductivity. This study attributes this conductivity difference to the phase-separated well-connected ionic channel morphology of the

block copolymer as evidenced by TEM. Similar to the results observed in proton conducting sulfonated block copolymers, all studies to date on hydroxide conducting block copolymers exhibit higher conductivity than their analogous random copolymers due to the microphase separated morphology in block copolymers.

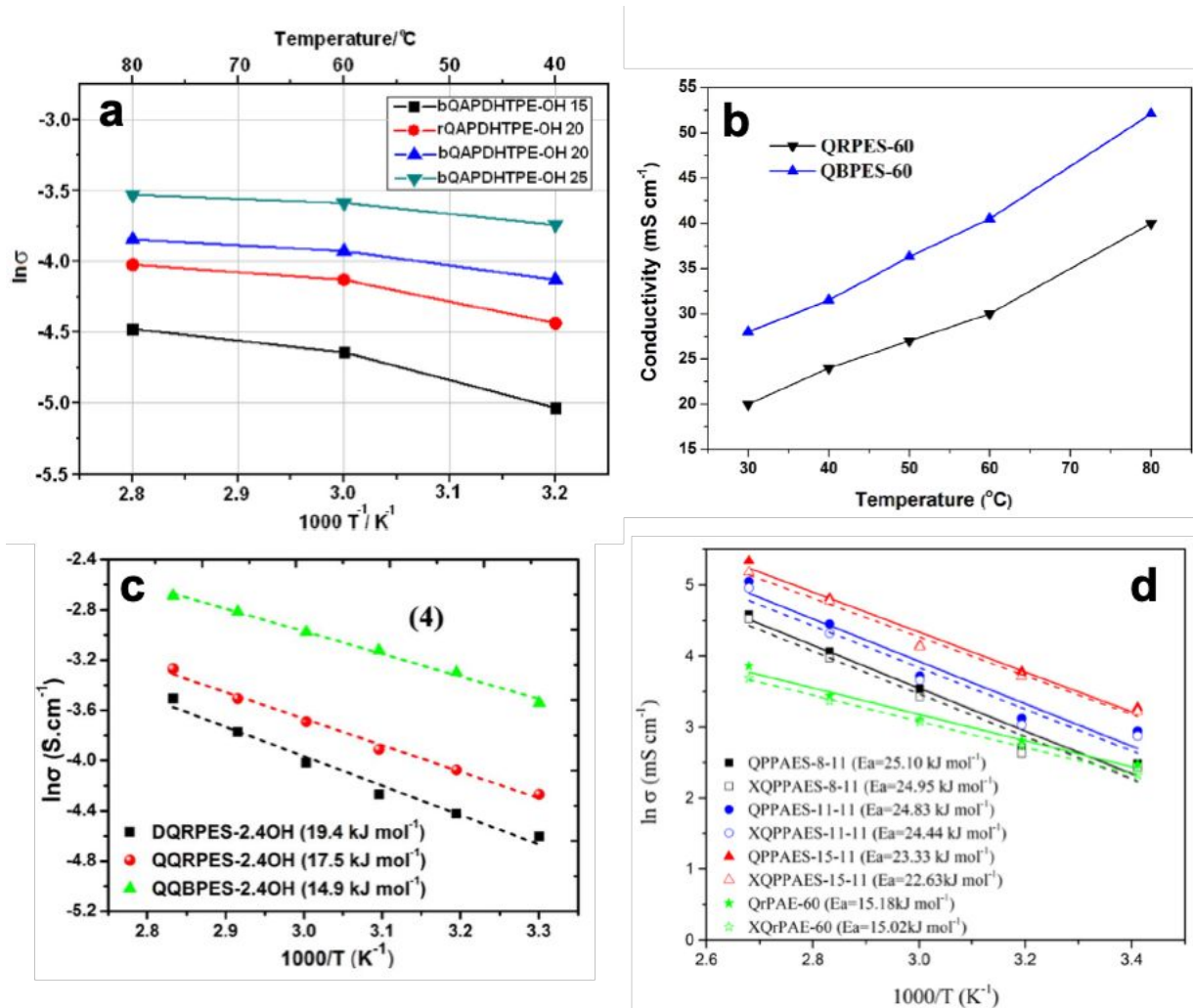


Figure 3. Examples of hydroxide ion conductivity of block and random copolymers: (a) poly(arylene ether sulfone) block (bQAPDHTPE) and random (rQAPDHTPE) copolymers with 4-4'-(2,2-diphenylenethenylidene) and quaternary ammonium cations, (b) cardo poly(arylene ether sulfone) block (QBPEs) and random (QRPEs) copolymers with bis-quaternary ammonium cations, (c) poly(arylene ether sulfone) block (QBPES) and random (QQRPEs, DQRPEs) copolymers di- (DQRPEs) and tetra-pyrrolidinium (QQRPEs, QQBPEs) cations, (d) crosslinkable fluorinated poly(arylene ether sulfone) block (QPPAES, XQPPAES) and random

(QrPAE, XQrPAE) copolymer with bis-quaternary ammonium cations. Figures adapted from refs. [16, 28, 35, 46].

4. Block Copolymers *versus* Polymer Blends

In addition to comparing block copolymers with random copolymers, Knauss, Herring, Lieratore and coworkers²⁶ examined a styrene-based block copolymer with ammonium-based cations and compared their properties to the analogous blend of the two polymers. Figure 4 shows the chloride ion conductivity of polystyrene-*b*-poly(vinylbenzyl trimethylammonium chloride) (PS-*b*-[PVBtMA][Cl]) diblock copolymer (see chemical structure in Fig 1e) and its analogous polymer blend polystyrene/poly(vinylbenzyl trimethylammonium chloride) (PS/[PVBtMA][Cl]). The conductivities were an order of magnitude higher for the block copolymer compared with the blend over the temperature range studied (50 - 90 °C) at various film thicknesses (40, 70, and 90 μm). Specifically, at 50 °C, the block copolymer possessed chloride conductivities of 24-33 mS cm⁻¹ compared to 0.7-6.0 mS cm⁻¹ for the blend. These differences were attributed to differences in morphology, where the block copolymer exhibited nanoscale phase separation as evidenced by SAXS (42 nm Bragg spacing) and the polymer blend exhibited micrometer scale phase separation as evidenced by optical microscopy (5 to 50 μm spherical regions). Figure 4 also highlights the impact of film thickness on the conductivity (a film thickness independent property for homogeneous isotropic materials), where changes in film thickness probably has a more significant impact on microscale morphology compared to nanoscale morphology. Overall, this study suggests that the domain size of the ionic regions have a significant impact on ion conductivity.

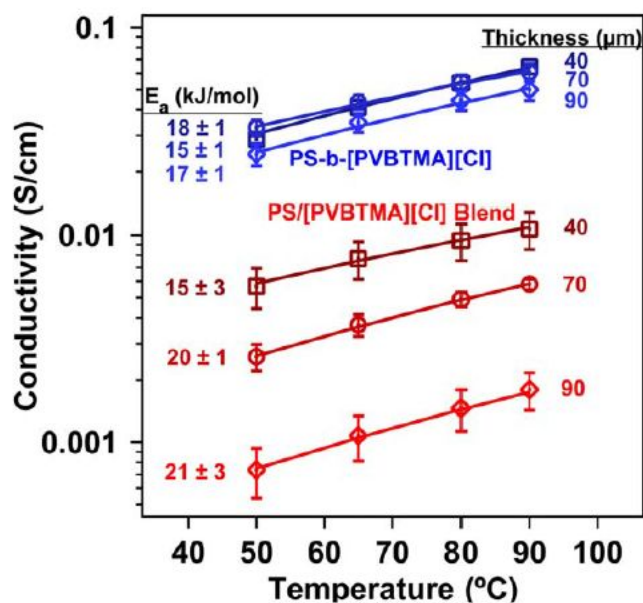


Figure 4. Example of chloride ion conductivity of block copolymer and analogous polymer blend: polystyrene-*b*-poly(vinylbenzyl trimethylammonium chloride) (PS-*b*-[PVBTMA][Cl]) diblock copolymer and polystyrene/poly(vinylbenzyl trimethylammonium chloride) (PS/[PVBTMA][Cl]) polymer blend. Figures adapted from ref. [26].

5. Block Copolymers *versus* Homopolymers

Similar to the studies in Figure 3, Elabd, Winey, and coworkers^{15,25} examined the hydroxide conductivity of a block copolymer with its analogous random copolymer, but also compared this with its analogous homopolymer. Figure 5 shows the temperature-dependent hydroxide ion conductivity of a methacrylate-based block copolymer with imidazolium-based cations (see chemical structure in Figure 1f) and its analogous random copolymer and homopolymer. At the same IEC (1.4 meq g⁻¹), the hydroxide conductivity of the block copolymer was an order of magnitude higher than its analogous random copolymer (at the same water content as well) (shown in Figure 5a) over the entire temperature range studied (30 – 80 °C). The difference in conductivity was attributed to the strong microphase separated lamellar morphology in the block copolymer as evidenced by SAXS, where no microphase separation was observed in the random copolymer. Interestingly, in Figure 5a, the hydroxide conductivity of the block copolymer was also higher than

its analogous homopolymer at the same experimental conditions, even though the homopolymer possessed a 3-fold higher IEC (4.2 meq g^{-1}) and a 2-fold higher water content compared to the block copolymer. Similar results (Figure 5b) were observed for the block copolymer with an IEC of 1.56 meq g^{-1} , but lower IECs (1.20 and 0.60 meq g^{-1}) resulted in lower conductivities than the homopolymer. Similar results were observed in another study by Elabd and coworkers,⁶⁷ where the bromide ion conductivity of a similar diblock copolymer (with longer alkyl side chains) was 3-fold higher than its analogous homopolymer. Bai and coworkers¹⁸ also observed similar results in their study on a poly(arylene ether sulfone)-*b*-poly(phenylene oxide)-based triblock copolymer with pendant ammonium cations, where a 6-fold increase in hydroxide conductivity was observed when comparing the triblock copolymer to its analogous homopolymer. Their study suggests that the microphase separated morphology for the triblock copolymer observed by SAXS improves conductivity compared to the homopolymer, where no microphase separation was observed for the homopolymer by SAXS. Overall, these results were unique and suggest that the ion-rich microdomains accelerate water-assisted ion transport in the block copolymer compared to the homopolymer. Both morphology factor analysis and percolation theory corroborated with the absolute conductivity results and the hypothesis that the local confinement of ions and water in ionic microdomains enhances conductivity.^{25, 67}

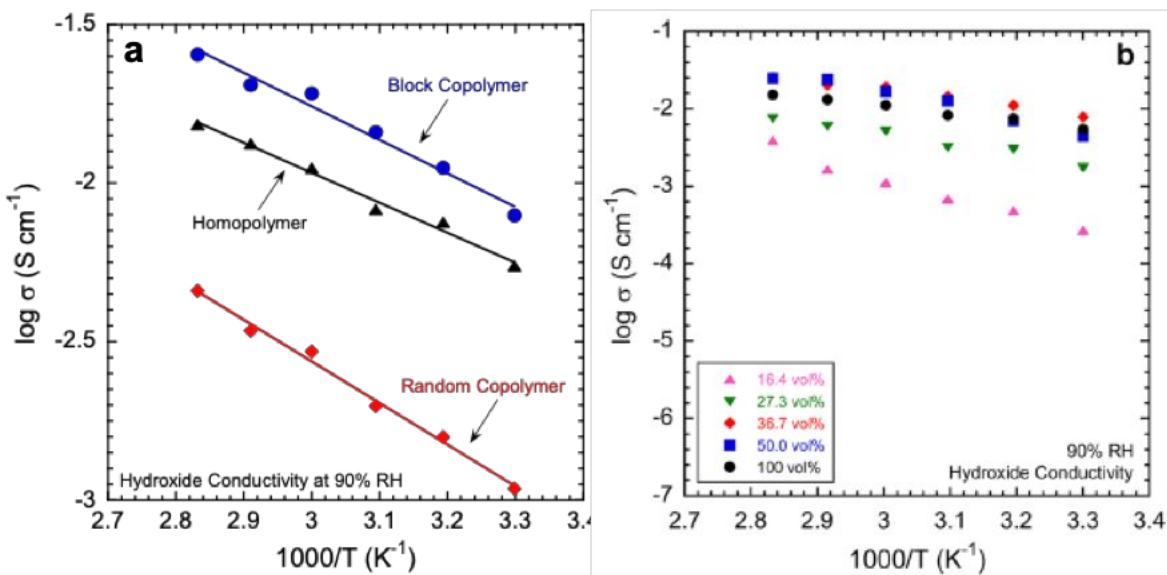


Figure 5. Example of temperature-dependent hydroxide conductivity in block copolymer poly(methyl methacrylate-*b*-1-[(2-methacryloyloxy)ethyl]-3-butylimidazolium hydroxide) [poly(MMA-*b*-MEBIm-OH)] and analogous homopolymer (poly(1-[(2-methacryloyloxy)ethyl]-3-butylimidazolium hydroxide) [poly(MEBIm-OH)]. Adapted from refs. [15, 25].

6. Block Copolymers with Short and Long Side Chains

Several studies have examined the impact of side chain length of the ion conductive block in a block copolymer (*i.e.*, the spacer length between the backbone and tethered pendant cation) on morphology and subsequently ion conductivity.^{32,53,48} Elabd and coworkers³² synthesized methacrylate-based block copolymers with imidazolium cations similar to the ones in Figure 5, but with longer alkyl side chains (undecyl or 11 carbons; $x = 11$) (see chemical structure in Figure 1g) and compared them to the ones in Figure 5 (ethyl or 2 carbons; $x = 2$). Figure 6a shows the bromide ion conductivity of these two block copolymers, where at a similar IEC, the block copolymer with longer alkyl side chains was 2-fold higher than the block copolymer with shorter alkyl side chains. Interestingly, the longer side chain block copolymer has a higher conductivity than the shorter side chain block copolymer (14.0 mS cm^{-1} versus 6.1 mS cm^{-1}) at a lower IEC (0.9 meq g^{-1} versus 1.4 meq g^{-1}) even though both polymers had the same block copolymer

morphologies (lamellar). One key difference, when saturated in liquid water, was that water/ion clusters were observed (in addition to the lamellar morphology) evidenced by both hydrated small-angle neutron scattering (SANS) and hydrated intermediate-angle X-ray scattering for the longer side chain block copolymer (and not for the one with shorter side chain block copolymer) with an intercluster distance on the order of 5 nm. Additionally, the hydrated SANS showed that the block copolymer morphology Bragg spacing for the longer side chain block copolymer (41.9 nm) was larger than the shorter side chain block copolymer (28.6 nm) at the same IEC (1.4 meq g⁻¹). This study shows that small chemical changes (alkyl side chain length) can induce the formation of water/ion clusters within block copolymer microdomains (localize the concentration and organization of ions) and increase the size of the block copolymer microdomains and subsequently significantly affect ion transport.

Figure 6b shows the temperature-dependent hydroxide ion conductivity for poly(arylene ether sulfone) block copolymers with long (Im-DFDM-bPES) (see chemical structure in Figure 1h) and short (Im-DFDB-bPES) side (aromatic) chains with tethered imidazolium cations, where the conductivity is higher for the longer side chain block copolymer compared to the shorter side chain block copolymer over the temperature range studied (25 – 80 °C). Specifically, at 80 °C in liquid water, the conductivities of the longer side chain block copolymer are 98.7 and 71.5 mS cm⁻¹ for IECs of 1.30 and 1.03 meq g⁻¹, respectively, while the conductivity of the shorter side chain block copolymer are 63.4 and 46.7 mS cm⁻¹ for IECs of 1.13 and 0.83 meq g⁻¹, respectively. In this study, both block copolymers exhibited well-defined microphase separation as evidenced by both AFM and TEM. The authors attribute this increase in conductivity to a larger hydrophilic phase size in the longer side chain block copolymer compared to the shorter side chain block copolymer (17-10 nm compared to 11-8 nm, respectively).

Figure 6c shows the temperature-dependent bicarbonate ion conductivity for poly(styrene-*b*-polybutadiene-*b*-polystyrene)) triblock copolymers with long (SBS-*c*-QA) and short (SBS-QA) side chains (on the midblock) with tethered quaternary ammonium cations (see chemical structure in Figure 1i). At 80 °C in liquid water, the longer side chain block copolymer has slightly higher bicarbonate conductivity (20.5 mS cm^{-1}) compared to the shorter side chain block copolymer (19.4 mS cm^{-1}) even though the longer side chain block copolymer has a significantly smaller IEC and water uptake (1.08 meq g^{-1} and 18.0 wt\% versus 2.30 meq g^{-1} and 57.1 wt\%). In this study, the morphology of the shorter side chain block copolymer is not presented. The SAXS data reveals a microphase separated morphology for the longer side chain block copolymer; one broad peak with a Bragg spacing of 48 nm , which was larger than the Bragg spacing observed prior to attaching the cation to the polymer (25 nm).

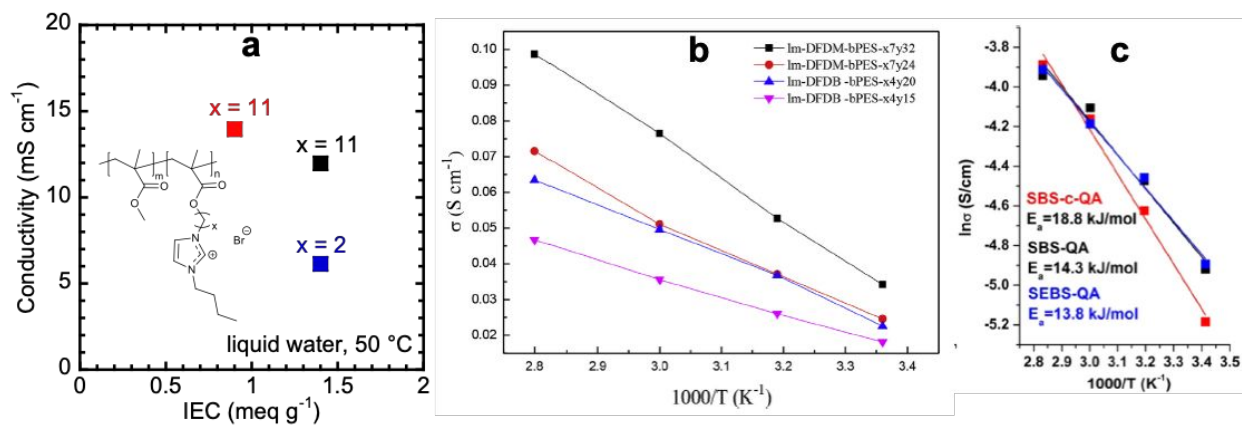


Figure 6. Examples of ion conductivity of block copolymers with short and long side chains: (a) bromide ion conductivity versus IEC for methacrylate-based diblock copolymer with imidazolium cations with both long (undecyl; 11 carbons; $x = 11$) and short (ethyl; 2 carbons; $x = 2$) alkyl spacer chain lengths, (b) temperature-dependent hydroxide ion conductivity for poly(arylene ether sulfone) block copolymers with long (Im-DFDM-bPES) and short (Im-DFDB-bPES) side (aromatic) chains with tethered imidazolium cations, (c) temperature-dependent bicarbonate ion conductivity for poly(styrene-*b*-polybutadiene-*b*-polystyrene)) triblock copolymers with long (SBS-*c*-QA) and short (SBS-QA) side chains (on the midblock) with tethered quaternary ammonium cations. Figures adapted from refs. [32, 53, 48].

7. Hydroxide Ion Conductivity *versus* Morphology Type

Figure 7 shows the morphologies of triblock and diblock copolymers of poly(chloromethyl styrene-*r*-styrene)-*b*-poly(isoprene) [P(CMS-*ran*-St)-*b*-Pip] with benzyl tris(2,4,6-tremethoxyphenyl)phosphonium (BzAr₃P⁺) cations (see chemical structure in Fig 1j) from a study by Beyer, Liberatore, Herring, Coughlin and coworkers.³³ Specifically, the SAXS profiles and an illustration of the two morphologies: lamellar and hexagonal phases are shown in Figures 7a and 7b, respectively.³³ At a similar IEC (0.44 and 0.45 meq g⁻¹ for triblock (AEM 2) and diblock (AEM 8), respectively), the chloride ion conductivity of the diblock was higher than the triblock at 95% RH and at all temperature studied (50, 65, 80, 90 °C). For example, at 90 °C and 95% RH, the conductivity of the diblock (20.6 mS cm⁻¹) was 3-fold higher than the triblock (6.9 mS cm⁻¹). This was attributed to the difference in morphology type (shown in Figure 7), where the triblock possessed a pseudo-2D lamellar morphology compared to the diblock 3D continuous morphology of hexagonally packed cylinders (where the cylinders are the non-conductive block). This study suggests that the ability for the ions to move freely in any direction (3D) reduces tortuosity and improves ion mobility.

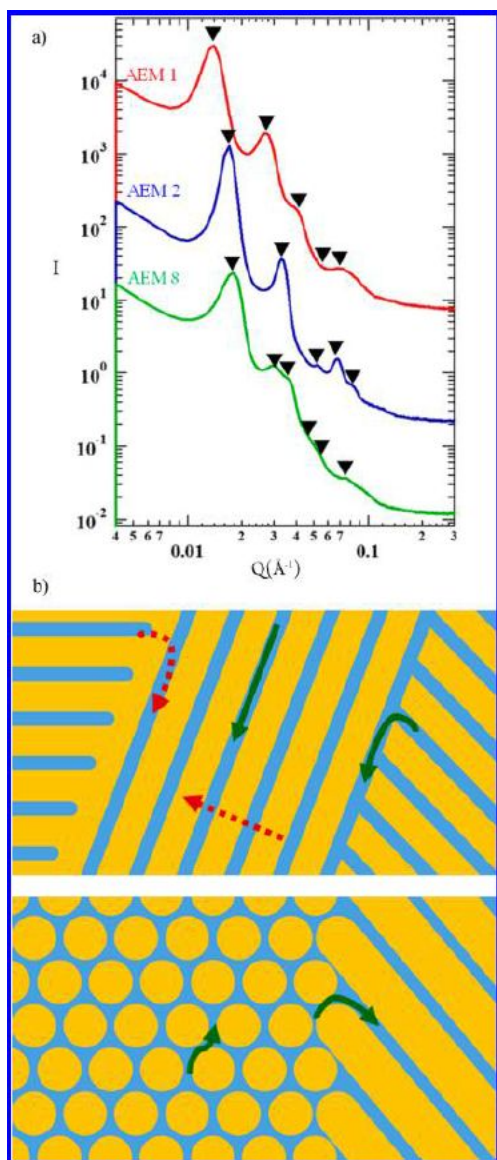


Figure 7. Morphologies of triblock and diblock copolymers of poly(chloromethyl styrene-*r*-styrene)-*b*-poly(isoprene) [P(CMS-*ran*-St)-*b*-Pip] with benzyl tris(2,4,6-tremethoxyphenyl)phosphonium (BzAr3P⁺) cations: (a) Small-angle X-ray scattering and (b) illustration of lamellar and hexagonal phases. Figure adapted ref. [33].

8. Conclusions

The benefits of the block copolymer chain architecture as AEMs for AFCs have been highlighted. Specifically, the phase separated morphologies of hydroxide conducting block copolymers have been shown to significantly improve hydroxide ion conductivity compared to

analogs of random copolymers, blends, and homopolymers. Furthermore, changes in morphology type and domain size (*via* side chain length) have also been shown to impact hydroxide ion conductivity. Similar to proton conducting sulfonated block copolymers, the morphology of hydroxide conducting block copolymers shows strong phase separation for both aromatic and aliphatic backbone block copolymers, where only the latter showed ordered periodic structures; however, periodicity does not seem to be a requirement for high hydroxide ion conductivity (see Table 1). Dissimilar to proton conducting sulfonated block copolymers, where only sulfonic acid based anions and protons (cations) have mostly been explored, research in hydroxide conducting block copolymers has pursued a variety of covalently tethered cations (*e.g.*, ammonium, imidazolium, pyrrolidinium, piperidinium, guanidinium, phosphonium) and counter mobile anions (*e.g.*, chloride, bromide, fluoride, bicarbonate) due to issues with alkaline chemical stability and ion exchange due to carbonation. Although various cation chemistries have been pursued (and cation/backbone/side chain pairings) with the goal of increasing alkaline chemical stability to improve long-lasting AFC performance (*i.e.*, must withstand the AFC environment of high pH at 80 °C), there are still few studies that include both *ex situ* chemical stability and *in operando* AFC time-dependent performance in the same study. Future studies that include both *ex situ* and *in operando* results will be of great interest in the advancement of solid-state AFCs.

Overall, it is clear that phase separated morphologies impact ion transport and the ability to combine orthogonal properties (high ion transport and high mechanical strength) in one material provides the potential to produce commercial robust thin AEMs that could be utilized to ensure high-power long-lasting AFCs. To realize these materials advances for AFCs, a more thorough fundamental understanding of predicting and controlling morphology in hydroxide conducting

block copolymers of various chemistries and chain architectures (to date, only diblock copolymers, triblock copolymers, and pentablock terpolymers have been explored) should be pursued.

Acknowledgements

This work is supported in part by the National Science Foundation under grant number CBET-1703645. Y.A.E. gratefully acknowledges the assistance of R. Sun on Figures 1 and 2.

References

1. Y. A. Elabd and M. A. Hickner, *Macromolecules*, 2011, **44**, 1-11.
2. Y. Liu, K. A. Cavicchi, J. Mausar and B. Decker, *Abstr Pap Am Chem S*, 2009, **237**.
3. Q. H. Zeng, Q. L. Liu, I. Broadwell, A. M. Zhu, Y. Xiong and X. P. Tu, *J Membrane Sci*, 2010, **349**, 237-243.
4. K. M. Lee, R. Wycisk, M. Litt and P. N. Pintauro, *J Membrane Sci*, 2011, **383**, 254-261.
5. M. Tanaka, K. Fukasawa, E. Nishino, S. Yamaguchi, K. Yamada, H. Tanaka, B. Bae, K. Miyatake and M. Watanabe, *J Am Chem Soc*, 2011, **133**, 10646-10654.
6. X. H. Li, Y. F. Yu, Q. F. Liu and Y. Z. Meng, *J Membrane Sci*, 2013, **436**, 202-212.
7. H. Ono, J. Miyake, B. Bae, M. Watanabe and K. Miyatake, *B Chem Soc Jpn*, 2013, **86**, 663-670.
8. D. Y. Park, P. A. Kohl and H. W. Beckham, *J Phys Chem C*, 2013, **117**, 15468-15477.
9. S. C. Price, X. M. Ren, A. C. Jackson, Y. S. Ye, Y. A. Elabd and F. L. Beyer, *Macromolecules*, 2013, **46**, 7332-7340.
10. A. H. N. Rao, H. J. Kim, S. Nam and T. H. Kim, *Polymer*, 2013, **54**, 6918-6928.
11. A. H. N. Rao, R. L. Thankamony, H. J. Kim, S. Nam and T. H. Kim, *Polymer*, 2013, **54**, 111-119.
12. N. T. Rebeck, Y. F. Li and D. M. Knauss, *J Polym Sci Pol Phys*, 2013, **51**, 1770-1778.
13. G. Sudre, S. Inceoglu, P. Cotanda and N. P. Balsara, *Macromolecules*, 2013, **46**, 1519-1527.
14. T. H. Tsai, A. M. Maes, M. A. Vandiver, C. Versek, S. Seifert, M. Tuominen, M. W. Liberatore, A. M. Herring and E. B. Coughlin, *J Polym Sci Pol Phys*, 2013, **51**, 1751-1760.
15. Y. S. Ye, S. Sharick, E. M. Davis, K. I. Winey and Y. A. Elabd, *Acs Macro Letters*, 2013, **2**, 575-580.
16. M. A. Hossain, Y. Lim, S. Lee, H. Jang, S. Choi, Y. Jeon, J. Lim and W. G. Kim, *Int J Hydrogen Energ*, 2014, **39**, 2731-2739.
17. H. C. Lee, K. L. Liu, L. D. Tsai, J. Y. Lai and C. Y. Chao, *Rsc Adv*, 2014, **4**, 10944-10954.
18. Q. Li, L. Liu, Q. Q. Miao, B. K. Jin and R. K. Bai, *Polym Chem-Uk*, 2014, **5**, 2208-2213.
19. X. H. Li, Q. F. Liu, Y. F. Yu and Y. Z. Meng, *J Membrane Sci*, 2014, **467**, 1-12.

20. Y. F. Li, A. C. Jackson, F. L. Beyer and D. M. Knauss, *Macromolecules*, 2014, **47**, 6757-6767.
21. J. Miyake, K. Fukasawa, M. Watanabe and K. Miyatake, *J Polym Sci Pol Chem*, 2014, **52**, 383-389.
22. J. R. Nykaza, Y. S. Ye and Y. A. Elabd, *Polymer*, 2014, **55**, 3360-3369.
23. N. Yokota, H. Ono, J. Miyake, E. Nishino, K. Asazawa, M. Watanabe and K. Miyatake, *Acs Appl Mater Inter*, 2014, **6**, 17044-17052.
24. Y. F. Li, Y. Liu, A. M. Savage, F. L. Beyer, S. Seifert, A. M. Herring and D. M. Knauss, *Macromolecules*, 2015, **48**, 6523-6533.
25. K. M. Meek, S. Sharick, Y. S. Ye, K. I. Winey and Y. A. Elabd, *Macromolecules*, 2015, **48**, 4850-4862.
26. M. A. Vandiver, B. R. Caire, Z. Poskin, Y. F. Li, S. Seifert, D. M. Knauss, A. M. Herring and M. W. Liberatore, *J Appl Polym Sci*, 2015, **132**.
27. C. G. Arges, Y. Kambe, H. S. Suh, L. E. Ocola and P. F. Nealey, *Chem Mater*, 2016, **28**, 1377-1389.
28. X. Dong, S. H. Hou, H. C. Mao, J. F. Zheng and S. B. Zhang, *J Membrane Sci*, 2016, **518**, 31-39.
29. Y. Hu, D. W. Gu, F. Li, X. C. Qi, K. H. Yang, X. D. Liu, H. Li and Y. M. Zhang, *J Mater Sci*, 2016, **51**, 5834-5842.
30. L. S. Liu, J. Ahlfield, A. Tricker, D. Chu and P. A. Kohl, *J Mater Chem A*, 2016, **4**, 16233-16244.
31. J. R. Nykaza, R. Benjamin, K. M. Meek and Y. A. Elabd, *Chem Eng Sci*, 2016, **154**, 119-127.
32. J. R. Nykaza, Y. S. Ye, R. L. Nelson, A. C. Jackson, F. L. Beyer, E. M. Davis, K. Page, S. Sharick, K. I. Winey and Y. A. Elabd, *Soft Matter*, 2016, **12**, 1133-1144.
33. W. Zhang, Y. Liu, A. C. Jackson, A. M. Savage, S. P. Ertem, T. H. Tsai, S. Seifert, F. L. Beyer, M. W. Liberatore, A. M. Herring and E. B. Coughlin, *Macromolecules*, 2016, **49**, 4714-4722.
34. P. Cotanda, N. Petzetakis, X. Jiang, G. Stone and N. P. Balsara, *J Polym Sci Pol Chem*, 2017, **55**, 2243-2248.
35. X. Dong, D. Lv, J. F. Zheng, B. X. Xue, W. H. Bi, S. H. Li and S. B. Zhang, *J Membrane Sci*, 2017, **535**, 301-311.
36. X. Dong, B. X. Xue, H. D. Qian, J. F. Zheng, S. H. Li and S. B. Zhang, *J Power Sources*, 2017, **342**, 605-615.
37. S. P. Ertem, B. R. Caire, T. H. Tsai, D. Zeng, M. A. Vandiver, A. Kusoglu, S. Seifert, R. C. Hayward, A. Z. Weber, A. M. Herring, E. B. Coughlin and M. W. Liberatore, *J Polym Sci Pol Phys*, 2017, **55**, 612-622.
38. E. Kim, S. Lee, S. Woo, S. H. Park, S. D. Yim, D. Shin and B. Bae, *J Power Sources*, 2017, **359**, 568-576.
39. C. X. Lin, X. Q. Wang, E. N. Hu, Q. Yang, Q. G. Zhang, A. M. Zhu and Q. L. Liu, *J Membrane Sci*, 2017, **541**, 358-366.
40. H. N. Sarode, Y. Yang, A. R. Motz, Y. F. Li, D. M. Knauss, S. Seifert and A. M. Herring, *J Phys Chem C*, 2017, **121**, 2035-2045.
41. D. J. Strasser, B. J. Graziano and D. M. Knauss, *J Mater Chem A*, 2017, **5**, 9627-9640.
42. Z. Y. Wang, J. Parrondo and V. Ramani, *J Electrochem Soc*, 2017, **164**, F1216-F1225.

43. X. L. Zhang, P. Chen, Q. Shi, S. S. Li, F. X. Gong, X. B. Chen and Z. W. An, *Int J Hydrogen Energ*, 2017, **42**, 26320-26332.
44. M. Zhu, M. Zhang, Q. Chen, Y. X. Su, Z. J. Zhang, L. Liu, Y. G. Wang, L. N. An and N. W. Li, *Polym Chem-Uk*, 2017, **8**, 2074-2086.
45. J. Y. Chu, K. H. Lee, A. R. Kim and D. J. Yoo, *Polymers-Basel*, 2018, **10**.
46. R. He, P. S. Wen, H. N. Zhang, S. M. Guan, G. Y. Xie, L. Z. Li, M. H. Lee and X. D. Li, *J Membrane Sci*, 2018, **556**, 73-84.
47. L. Liu and P. A. Kohl, *J Polym Sci Pol Chem*, 2018, **56**, 1395-1403.
48. L. Liu, D. F. Li, Y. Xing and N. W. Li, *J Membrane Sci*, 2018, **564**, 428-435.
49. K. M. Meek, R. Sun, C. Willis and Y. A. Elabd, *Polymer*, 2018, **134**, 221-226.
50. A. K. Mohanty, S. Devaraju, N. Kim and H. J. Paik, *Solid State Ionics*, 2018, **314**, 46-56.
51. S. K. Tuli, A. L. Roy, R. A. Elgammal, M. K. Tian, T. A. Zawodzinski and T. Fujiwara, *J Membrane Sci*, 2018, **565**, 213-225.
52. K. B. Zhang, S. T. Gong, B. L. Zhao, Y. X. Liu, N. A. Qaisrani, L. D. Li, F. X. Zhang and G. H. He, *J Membrane Sci*, 2018, **550**, 59-71.
53. X. L. Zhang, S. S. Li, P. Chen, J. J. Fang, Q. Q. Shi, Q. Weng, X. J. Luo, X. B. Chen and Z. W. An, *Int J Hydrogen Energ*, 2018, **43**, 3716-3730.
54. X. L. Zhang, Q. Shi, P. Chen, J. F. Zhou, S. S. Li, H. Xu, X. B. Chen and Z. W. An, *Polym Chem-Uk*, 2018, **9**, 699-711.
55. M. Zhu, X. J. Zhang, Y. G. Wang, Y. B. Wu, H. Wang, M. Zhang, Q. Chen, Z. C. Shen and N. W. Li, *J Membrane Sci*, 2018, **554**, 264-273.
56. J. R. Varcoe and R. C. T. Slade, *Fuel Cells*, 2005, **5**, 187-200.
57. G. Merle, M. Wessling and K. Nijmeijer, *J Membrane Sci*, 2011, **377**, 1-35.
58. M. R. Hibbs, M. A. Hickner, T. M. Alam, S. K. McIntyre, C. H. Fujimoto and C. J. Cornelius, *Chem Mater*, 2008, **20**, 2566-2573.
59. Y. A. Elabd, E. Napadensky, J. M. Sloan, D. M. Crawford and C. W. Walker, *J Membrane Sci*, 2003, **217**, 227-242.
60. Y. A. Elabd, C. W. Walker and F. L. Beyer, *J Membrane Sci*, 2004, **231**, 181-188.
61. K. M. Meek and Y. A. Elabd, *J Mater Chem A*, 2015, DOI: 10.1039/C5TA07170D.
62. Y. S. Ye and Y. A. Elabd, *Macromolecules*, 2011, **44**, 8494-8503.
63. K. M. Meek and Y. A. Elabd, *Macromolecules*, 2015, **48**, 7071-7084.
64. K. M. Meek, J. R. Nykaza and Y. A. Elabd, *Macromolecules*, 2016, **49**, 3382-3394.
65. Z. Sun, B. C. Lin and F. Yan, *Chemsuschem*, 2018, **11**, 58-70.
66. K. M. Meek and Y. A. Elabd, *J Mater Chem A*, 2015, **3**, 24187-24194.
67. J. R. Nykaza, Y. Ye and Y. A. Elabd, *Polymer*, 2014, **55**, 3360-3369.

